Structural Optimization of Triboelectric Nanogenerator for Harvesting Water Wave Energy

Tao Jiang,[†,§] Li Min Zhang,[†,§] Xiangyu Chen,[†] Chang Bao Han,[†] Wei Tang,[†] Chi Zhang,[†] Liang Xu,[†] and Zhong Lin Wang[*,†,‡]

[†]Beijing Institute of Nanoenergy and Nanosystems, Chinese Academy of Sciences, Beijing 100083, China and [‡]School of Materials Science and Engineering, Georgia Institute of Technology, Atlanta, Georgia 30332-0245, United States. [§]T.J. and L.M.Z. contributed equally to this work.

ABSTRACT Ocean waves are one of the most abundant energy sources on earth, but harvesting such energy is rather challenging due to various limitations of current technologies. Recently, networks formed by triboelectric nanogenerator (TENG) have been proposed as a promising technology for harvesting water wave energy. In this work, a basic unit for the TENG network was studied and optimized, which has a box structure composed of walls made of TENG composed of a wavy-structured Cu-Kapton-Cu film and two FEP thin films, with a metal ball enclosed inside. By combination of the theoretical calculations and experimental studies, the output performances of the TENG unit were investigated for various structural parameters, such as the size, mass, or number of the metal balls. From the viewpoint of theory, the output characteristics of TENG during its collision with the ball were numerically calculated by the finite element method and interpolation method, and there exists an optimum ball size or mass to reach maximized output power and electric energy. Moreover, the theoretical results were well verified by the experimental tests. The present work could provide guidance for structural optimization of wavy-structured TENGs for effectively harvesting water wave energy toward the dream of large-scale blue energy.

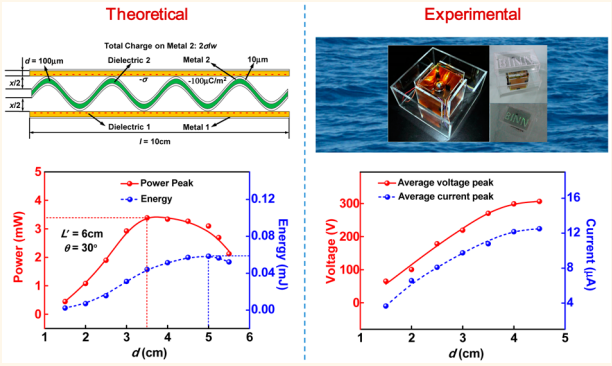

KEYWORDS: triboelectric nanogenerator · water wave energy · structural optimization · blue energy

With an increasing consumption of fossil fuels, humans will be threatened with serious energy crises. Searching for a new energy source from our ambient environment is of great practical value for the sustainable development of our society.[1] Because of the abundant water resources on the earth, ocean waves are one of the most promising renewable energy sources for large-scope applications. The wave energy exhibits superior advantages over other energy sources; for instance, it has a much less dependence on season, day or night, weather, and temperature conditions.[2,3] However, this type of water kinetic energy has rarely been exploited due to the lack of suitable energy scavenging technologies.[4,5] Most demonstrated converters for water waves rely on the electromagnetic generators that face huge challenges such as low turbine efficiency at ocean wave frequency and motion modes, seawater erosion of facilities, heavy weight, and the high cost of equipment maintenance and replacement.[6−8] Therefore, a small-sized, lightweight, cost-effective, and all-in-one approach for converting water wave energy into electricity is greatly desirable as a key to solve the above problems.

Recently, triboelectric nanogenerator (TENG) has emerged as a powerful technology for harvesting mechanical energy based on the coupling of triboelectrification and electrostatic induction, with unique merits of high power density, high efficiency, low weight and fabrication cost.[9−14] This technology has been applied to harvest energy from a variety of sources, such as human walking,[15] mechanical vibration,[16] rotation,[17] wind,[18] water waves,[19−21] and so on. Considering that the TENGs have obvious advantages over electromagnetic generators in harvesting energy from low-frequency movement, the TENG technology

* Address correspondence to zlwang@gatech.edu.

Received for review October 9, 2015 and accepted November 14, 2015.

Published online 10.1021/acsnano.5b06372

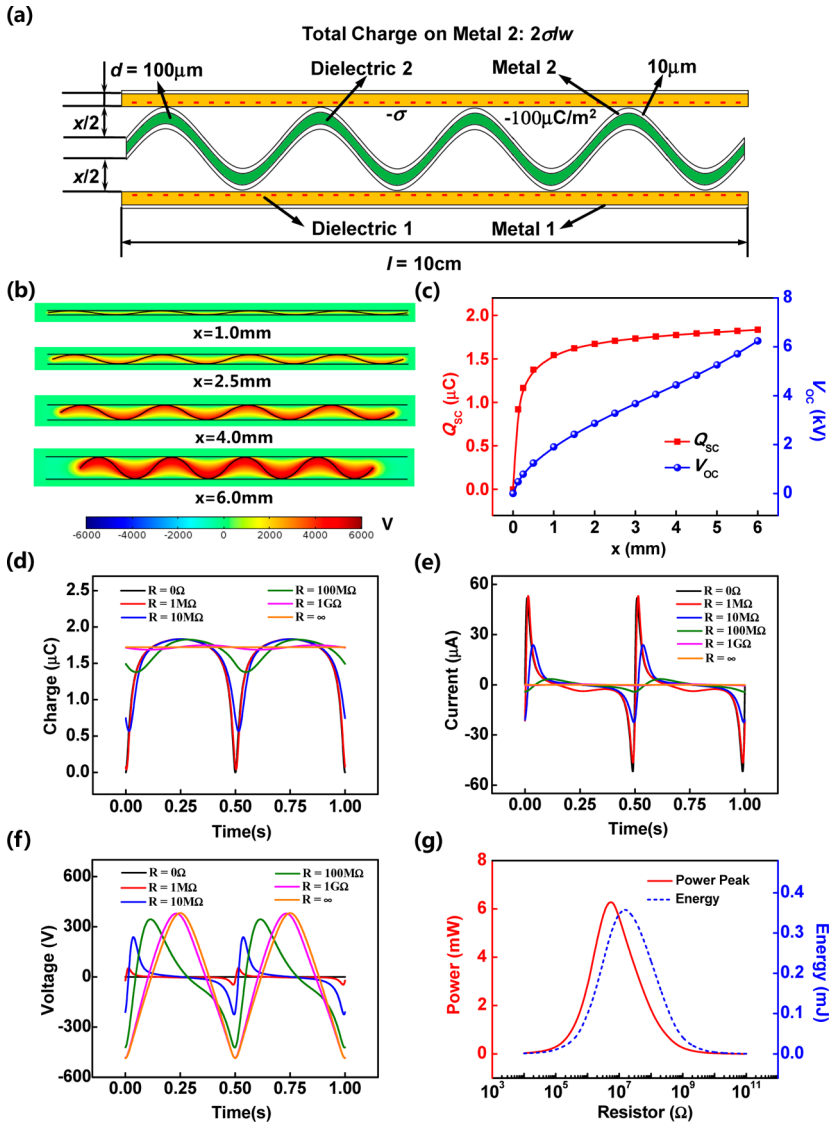

Figure 1. (a) FEM model of wavy-structured TENG. (b) Electric potential distribution under OC condition for different separation distance *x*. (c) Q_{SC} and V_{OC} as functions of *x*. (d–f) Charge-time, current–time and voltage–time relationships at different load resistances when imposed a periodic triggering with a frequency of 2 Hz. (g) Maximum output power and generated electric energy with load resistance.

could provide a new strategy for wave energy conversion and be of huge potential toward large-scale blue energy harvesting from the ocean. In our previous work, we reported a network design made of connected TENGs for large-scale harvesting of kinetic water energy.[22] The TENG networks that naturally float on the water surface can convert the slow, random, and high-force oscillatory wave energy into electricity. Nevertheless, the applications of TENG in wave energy utilization are still in the conceive stage, and more explorations are highly desired to optimize the structure and performance of TENG toward practical applications in blue energy.

In the present work, we designed a TENG with a wavy-structured conductor-dielectric-conductor film sandwiched between two flat dielectric films for harvesting water wave energy. Four such TENG units were anchored as standing walls of a box, inside which a free rolling ball was placed to collide with the walls once subjected to water wave disturbance. First, a theoretical model of the wavy-structured TENG was constructed, and its output characteristic when imposed a periodic triggering at a low frequency was investigated to simulate the impact of water waves. Then, the output performances of TENG during its collision with a metal ball in typical collision modes were numerically calculated by the finite element method (FEM) and interpolation method. The influences of structural parameters, such as the size, mass, or number of metal ball, were mainly addressed, providing a theoretical prediction for performance improvement of TENG in wave energy harvesting. Finally, to verify the theoretical results, real water wave tests were carried out using as-fabricated TENG devices, and the ball

size dependent output behavior was demonstrated. Combining the theoretical calculations and experimental studies, the strategies for structural optimization of TENGs in harvesting water wave energy were provided.

RESULTS AND DISCUSSION

The FEM model for a wavy-structured TENG was established with dimensions close to those of the real device, as shown in Figure 1a. Considering that the width w of whole structure (10 cm) is much larger than the thickness of the film (0.1 mm), a 2D model was utilized to simplify the calculation. Between two flat dielectric layers (Dielectric 1, $\varepsilon_{r1} = 2$, length $l = 10$ cm) bonded with metal electrodes (Metal 1), a wavy structure is sandwiched in which both sides of the middle dielectric layer (Dielectric 2, $\varepsilon_{r2} = 2$) are coated by Metal 2. The thicknesses of all dielectric and metal layers are 0.1 mm and 0.01 mm, respectively. The separation distance (x) is defined as the gap between two flat dielectric surfaces subtracted by the wavy core thickness. The charge densities at two tribo-surfaces of Dielectric 1 were assigned as $-\sigma$ (100 μC m^{-2}), and two wavy layers of Metal 2 have the positive charges of amount $2\sigma lw$ in total for charge conservation.

The FEM calculations under the short-circuit (SC) and open-circuit (OC) conditions were carried out by the COMSOL software. Two wavy layers of Metal 2 have the same potential as well as two flat layers of Metal 1 to reflect the electric connection. The detailed method can be found in our previous work.[23] The typical electric potential distributions for various separation distances x under OC condition are shown in Figure 1b. As x increases from 0 to maximum value ($x_m = 6$ mm), the potential difference between Metal 2 and Metal 1 gradually increases up to ~6 kV, and the open-circuit voltage V_{OC} increases (Figure 1c). Because such wavy-structured TENG can be self-restorable after impact and convert vertical compressing into lateral sliding,[21] the wavy core is extended in the vertical direction and retracted in the horizontal direction when x increases. In the calculations, we kept the wavy core having a fixed length. The short-circuit charge Q_{SC} was found to increase rapidly first with increasing x and then reach a saturation. The change in capacitance ($C = Q_{SC}/V_{OC}$) leads to a change in the field potential driving the electron flow in the external circuit, which is the general working mechanism of this TENG.

A previous work demonstrated that the wavy structure of the TENG can be easily packaged for harvesting the impact energy from water waves.[21] To simulate the impact of water waves, we imposed a periodic triggering at a low frequency on this TENG and further investigated its output characteristics. Similar to the literatures,[24−26] we established the $V-Q-x$ relationship for the wavy-structured TENG given by

$$V = -\frac{1}{C(x)} \times Q + V_{OC}(x) \tag{1}$$

where $1/C(x)$ and $V_{OC}(x)$ are obtained by the continuous fraction interpolation based on FEM results. The resistive load characteristics can be calculated by combining the semianalytical $V-Q-x$ relationship and Ohm's law through the following equation:

$$R\frac{dQ}{dt} = V = -\frac{1}{C(x)} \times Q + V_{OC}(x) \tag{2}$$

The differential equation can be solved by specifying the motion process (specified $x(t)$ profile) and the boundary condition. We adopted a harmonic motion mode to reflect a periodic triggering, and the $x-t$ relationship is mathematically given by[27]

$$x(t) = \frac{x_m}{2}(1 - \cos \omega t) \tag{3}$$

where $x_m = 6$ mm and angular frequency $\omega = 4\pi$ ($f = 2$ Hz). By applying the periodic boundary condition[26]

$$Q(t = 0) = Q\left(t = \frac{2\pi}{\omega}\right) \tag{4}$$

the steady-state output of wavy-structured TENG for arbitrary load resistance can be calculated. The equations for transferred charge Q are obtained as follows:

$$Q = \exp\left(-\int_0^t \frac{dt}{RC(x(t))}\right) \times \left[Q_0 + \int_0^t \frac{V_{OC}(x(t))}{R} \exp\left(\int_0^t \frac{dz}{RC(x(z))}\right) dt\right], \quad 0 \le t \le \frac{\pi}{\omega} \tag{5a}$$

$$Q = \exp\left(-\int_{\pi/\omega}^t \frac{dt}{RC(x(t))}\right) \times \left[Q\left(\frac{\pi}{\omega}\right) + \int_{\pi/\omega}^t \frac{V_{OC}(x(t))}{R} \exp\left(\int_{\pi/\omega}^t \frac{dz}{RC(x(z))}\right) dt\right], \quad \frac{\pi}{\omega} \le t \le \frac{2\pi}{\omega} \tag{5b}$$

where Q_0 is given by

$$Q_0 = \frac{\exp\left(-\frac{2}{R}\int_0^{\pi/\omega} \frac{dt}{C(x(t))}\right) \times \int_0^{\pi/\omega} \frac{V_{OC}(x(t))}{R} \exp\left(\int_0^t \frac{dz}{RC(x(z))}\right) dt + \int_0^{\pi/\omega} \frac{V_{OC}(x(t))}{R} \exp\left(-\int_0^t \frac{dz}{RC(x(t))}\right) dt}{1 - \exp\left(-\frac{2}{R}\int_0^{\pi/\omega} \frac{dt}{C(x(t))}\right)}$$

Through the differentiation of Q by t, we can obtain the equations of current I for arbitrary load resistance

$$I = \frac{V_{OC}(x(t))}{R} - \frac{\exp\left(-\int_0^t \frac{dt}{RC(x(t))}\right)}{RC(x(t))} \times \left[Q_0 + \int_0^t \frac{V_{OC}(x(t))}{R} \exp\left(\int_0^t \frac{dz}{RC(x(z))}\right) dt\right], \quad 0 \le t \le \frac{\pi}{\omega} \tag{6a}$$

$$I = \frac{V_{OC}(x(t))}{R} - \frac{\exp\left(-\int_{\pi/\omega}^t \frac{dt}{RC(x(t))}\right)}{RC(x(t))} \times \left[Q\left(\frac{\pi}{\omega}\right) + \int_{\pi/\omega}^t \frac{V_{OC}(x(t))}{R} \exp\left(\int_{\pi/\omega}^t \frac{dz}{RC(x(z))}\right) dt\right], \quad \frac{\pi}{\omega} \le t \le \frac{2\pi}{\omega} \tag{6b}$$

and then the voltage V can be calculated by the Ohm's law.

Figure 1d−f presents the real-time output charge, current, and voltage of the wavy-structured TENG when imposed the periodic triggering of 2 Hz. Periodic waves with a period of $2\pi/\omega$ (0.5 s) are obtained for all $Q-t$, $I-t$, and $V-t$ curves. The current and voltage are both AC signals, and their time integrations in one cycle are zero. At SC condition and small R, the transfer charge increases rapidly to its saturation and drops at the end of one cycle, leading to two sharp peaks for the current. With increasing R, the oscillation magnitude of Q curve decreases gradually until 0 due to the increasing limitation of charge transport. The peak of current decreases, while the peak of voltage increases, indicating a three-working-region behavior. In the middle range of R, the peak transit power is reached and the maximum energy from a single cycle can be reached as well (Figure 1g), with the two corresponding optimum resistances approaching one another. The numerical results demonstrate that the wavy-structured TENG can work well to harvest energy from periodic triggering including a water wave impact.

In this work, we harvested the water wave energies mainly by means of the collision between a metal ball and TENG walls, thus it is necessary to understand the electric output behavior of TENG during the collision. At the initial state, the wavy-structured TENG has the maximum separation distance (x_m = 6 mm). This state under SC condition was chosen as the charge reference state, and the Q_{SC} was calculated as the total transferred charges under SC ($Q_{net,SC}$) subtracted by the charge at such reference state, similar to the reported work.[23] The V_{OC} was recalculated by $V_{OC} = Q_{SC}/C$. We defined the compression deformation depth as x_1 for avoiding confusion with the separation distance x. On the basis of the governing equation of TENG (eq 2), as long as the $x_1(t)$ is specified, the output characteristics can be numerically calculated by interpolation and solving of differential equation.[25,26] We assumed that the wavy-structured film can be considered as an ideal harmonic spring. It is known that the film can be easily compressed first, and the compression becomes more difficult when a certain deformation depth is achieved. This is similar to the compression limit of a spring, after which a further compression can destroy the spring. But our polymer film coated by metal electrodes can be still compressed until a complete contact, and the wavy structure can be fully recovered after the collision. Therefore, we set a smaller spring constant k_1 = 2 N/mm before a critical compression depth x_{1c} (chosen as 4.5 mm in the calculations) and a larger spring constant k_2 = 50 N/mm after the x_{1c}. According to the force analysis and motion equation, we can calculate the $x_1(t)$ equation at different time ranges, and then the electric properties.

A horizontal collision mode was first designed, as shown in Figure 2a. The metal ball is rolling at the center of a box to collide with the TENG walls on both sides. The cubic structure with a length of L = 10 cm is fixed and anchored at the horizontal plane. When given a constant impulse (triggering), the metal ball can possess a constant momentum. The increase of ball size (diameter d) can bring the increase of ball mass ($m = \rho\pi d^3/6$, ρ = 7.9 g/cm^3) and decrease of initial velocity v_0 of the ball. The surface of rolling orbit for the ball is assumed to be smooth without friction. When the ball collides with the acrylic plate (mass $m_0 = \rho_0 V_0$ = 12 g, ρ_0 = 1.2 g/cm^3) on the TENG surface, the momentum is conserved but there is energy loss due to the internal energy change. The collision can be considered as a completely inelastic collision, and the ball and the acrylic have the same velocity of $v_1 = mv_0/(m + m_0)$ after the collision. During one collision, the metal ball first compresses the TENG to the maximum depth x_{1m}, and then the ball is rebounded until it is separated from the acrylic surface. When the TENG is recovered to initial undeformed balance position ($x_1 = 0$), further extension is forbidden due to the restriction of an adhesive tape in real device. On the basis of Newton's second law and Hooke's law, the $x_1(t)$ equations were derived for two cases of $x_{1m} \le x_{1c}$ (maximum compression within the transition point of spring constant) and $x_{1m} > x_{1c}$ (maximum compression beyond the transition point). For $x_{1m} \le x_{1c}$, the $x_1(t)$ is given by

$$x_1(t) = v_1\sqrt{\frac{m+m_0}{k_1}}\sin\sqrt{\frac{k_1}{m+m_0}}t \tag{7}$$

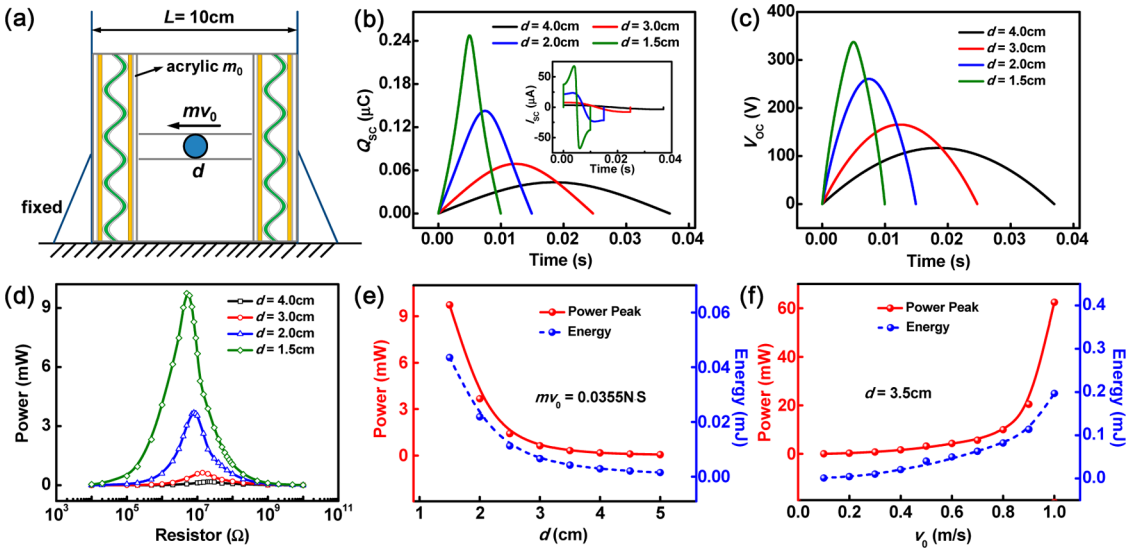

Figure 2. (a) Schematic representation of the horizontal collision between the metal ball and TENG in the device. (b,c) Q_{SC}, I_{SC}, and V_{OC} as functions of time for various ball diameters d when given a constant momentum. (d) Maximum output power with respect to resistance for various d. (e) Effect of ball diameter on the maximum power and electric energy at a constant momentum. (f) Power and electric energy for various v_0 at a fixed d (3.5 cm).

For $x_{1m} > x_{1c}$, the $x_1(t)$ is given by

$$x_1(t) = v_1\sqrt{\frac{m+m_0}{k_1}}\sin\sqrt{\frac{k_1}{m+m_0}}t, \quad 0\le t\le t_c \tag{8a}$$

$$x_1(t) = v_c\sqrt{\frac{m+m_0}{k_2}}\sin\sqrt{\frac{k_2}{m+m_0}}(t-t_c) + \frac{k_1x_{1c}}{k_2}\cos\sqrt{\frac{k_2}{m+m_0}}(t-t_c) - \frac{k_1x_{1c}}{k_2}+x_{1c}, \quad t_c\le t\le 2t_m-t_c \tag{8b}$$

$$x_1(t) = -v_c\sqrt{\frac{m+m_0}{k_1}}\sin\sqrt{\frac{k_1}{m+m_0}}(t-2t_m+t_c) + x_{1c}\cos\sqrt{\frac{k_1}{m+m_0}}(t-2t_m+t_c), \quad 2t_m-t_c\le t\le 2t_m \tag{8c}$$

where the velocity v_c at the x_{1c} is given by $v_c = (v_1^2 - (k_1/(m+m_0))x_{1c}^2)^{1/2}$, and the time t_c and t_m when compressed to the x_{1c} and x_{1m} are given by

$$t_c = \sqrt{\frac{m+m_0}{k_1}}\arcsin\frac{x_{1c}}{v_1}\sqrt{\frac{k_1}{m+m_0}},$$

$$t_m = \sqrt{\frac{m+m_0}{k_2}}\arctan\frac{v_c\sqrt{(m+m_0)k_2}}{k_1x_{1c}}+t_c$$

For a detailed derivation, see Supporting Information, Section 1.

After specifying the $x_1(t)$ equations, we can obtain the dynamic output characteristic equations for the wavy-structured TENG during its collision with the metal ball. We take the case of $x_{1m} \le x_{1c}$ for example. By applying a boundary condition of Q (t = 0) = 0, the $Q-t$, $I-t$, $V-t$ relationship equations are presented as follows:

$$Q = \frac{1}{R}\exp\left(-\int_0^t\frac{dt}{RC(x_1(t))}\right)\int_0^t V_{OC}(x_1(t))\exp\left(\int_0^t\frac{dz}{RC(x_1(z))}\right)dt \tag{9}$$

$$I = \frac{V_{OC}(x_1(t))}{R} - \frac{1}{R^2C(x_1(t))}\exp\left(-\int_0^t\frac{dt}{RC(x_1(t))}\right)\times\int_0^t V_{OC}(x_1(t))\exp\left(\int_0^t\frac{dz}{RC(x_1(z))}\right)dt \tag{10}$$

$$V = V_{OC}(x_1(t)) - \frac{1}{RC(x_1(t))}\exp\left(-\int_0^t\frac{dt}{RC(x_1(t))}\right)\times\int_0^t V_{OC}(x_1(t))\exp\left(\int_0^t\frac{dz}{RC(x_1(z))}\right)dt \tag{11}$$

For the case of $x_{1m} > x_{1c}$, the Q, I, V should be calculated successively for the three time ranges. The charge Q at the end of last time range is the initial boundary condition for next time range. After the collision ($t > 2t_m$), the wavy structure is fully recovered to its initial state, and the Q, I, V start to decay exponentially. The formula derivations and details can be found in Section 2 of Supporting Information.

Figure 2b,c shows the real-time Q_{SC}, I_{SC}, and V_{OC} for various ball diameters d in one horizontal collision when given a constant momentum mv_0 = 0.0355 N·s (v_0 = 0.2 m/s for d = 3.5 cm). As can be seen, the Q_{SC} and V_{OC} curves both have the parabolic shape with symmetry about the maximum compression depth. When the ball size increases, the maximum values of Q_{SC} and V_{OC} both decrease, but the lasting time of collision becomes longer due to the lower ball velocity.

From the inset of Figure 2b, we can also view the decrease of I_{SC} with increasing d. Then we calculated the dynamic output characteristics of TENG during one collision, *i.e.*, the $Q-t$, $I-t$, $V-t$ relationship for various R. The current and voltage peak values clearly indicate the three-working-region behavior, and the optimum resistance for the maximum transit power is observed (Figure S1). The dependences of maximum power and generated electric energy on the ball size during one collision were also examined. The power with respect to R for various d are shown in Figure 2d, revealing that the TENG can transit higher power at a relatively lower matched resistance for smaller d. As well as the power peak value, the electric energy decreases gradually with the increase of ball diameter (Figure 2e). Note that the above results can only represent the collision-induced output behavior of TENG when the metal ball undergoes a constant impulse. In addition, for a fixed ball size (*e.g.*, d = 3.5 cm), the effect of initial ball velocity v_0 on the power and energy was studied. The power and energy were found to increase with increasing v_0, as shown in Figure 2f. That is because a larger v_0 can lead to a faster compression and a larger deformation depth.

Besides the horizontal collision, the vertical collision was also discussed, whose sketch is shown in Figure 3a. The metal ball with a zero initial velocity starts to drop under the gravity force and collide with the center position of the TENG. The drag force of air is neglected. When changing the ball size, we keep the top of metal ball at the same height h above the acrylic surface. This is to consider the restricted moving space for the metal ball in a real device. The ball velocity when it gets the acrylic surface is defined as v_0, and the velocity after its collision with the acrylic is defined as v_1. Since there is only the gravity force, the collision is still regarded as a completely inelastic collision, and the ball and acrylic have the same velocity v_1. For this collision mode taking the gravity force into account, the $x_1(t)$ equations were also derived for $x_{1m} \le x_{1c}$ and $x_{1m} > x_{1c}$. For $x_{1m} \le x_{1c}$, the $x_1(t)$ equation is given by

$$x_1(t) = v_1\sqrt{\frac{m+m_0}{k_1}}\sin\sqrt{\frac{k_1}{m+m_0}}t - \frac{(m+m_0)g}{k_1}\cos\sqrt{\frac{k_1}{m+m_0}}t + \frac{(m+m_0)g}{k_1} \quad (12)$$

For the case of $x_{1m} > x_{1c}$, when $0 \le t \le t_c$, the $x_1(t)$ equation is the same as eq 12. When $t_c \le t \le 2t_m - t_c$ and $2t_m - t_c \le t \le 2t_m$, the $x_1(t)$ equation is obtained as follows (for details, see Section 1, Supporting Information):

$$x_1(t) = v_c\sqrt{\frac{m+m_0}{k_2}}\sin\sqrt{\frac{k_2}{m+m_0}}(t-t_c) - \frac{(m+m_0)g - k_1x_{1c}}{k_2}\cos\sqrt{\frac{k_2}{m+m_0}}(t-t_c) + \frac{(m+m_0)g - k_1x_{1c}}{k_2} + x_{1c}, \quad t_c \le t \le 2t_m - t_c \quad (13a)$$

$$x_1(t) = -v_c\sqrt{\frac{m+m_0}{k_1}}\sin\sqrt{\frac{k_1}{m+m_0}}(t-2t_m+t_c) + \frac{k_1x_{1c} - (m+m_0)g}{k_1}\cos\sqrt{\frac{k_1}{m+m_0}}(t-2t_m+t_c) + \frac{(m+m_0)g}{k_1}, \quad 2t_m - t_c \le t \le 2t_m \quad (13b)$$

where v_c, t_c, t_m are given by

$$t_c = \sqrt{\frac{m+m_0}{k_1}}\left[\arcsin\frac{k_1x_{1c} - (m+m_0)g}{\sqrt{(m+m_0)^2g^2 + (m+m_0)k_1{v_1}^2}} + \arcsin\frac{(m+m_0)g}{\sqrt{(m+m_0)^2g^2 + (m+m_0)k_1{v_1}^2}}\right]$$

$$v_c = \sqrt{{v_1}^2 + 2gx_{1c} - \frac{k_1}{m+m_0}{x_{1c}}^2},$$

$$t_m = \sqrt{\frac{m+m_0}{k_2}}\arctan\frac{v_c\sqrt{(m+m_0)k_2}}{k_1x_{1c} - (m+m_0)g} + t_c$$

After specifying the $x_1(t)$ equations, the dynamic output characteristics were calculated by using the above method (eqs 9−11, Section 2, Supporting Information)

The Q_{SC}, I_{SC}, and V_{OC} in one vertical collision when given a constant height h = 6 cm were calculated for various ball diameters d, as shown in Figure 3b,c. The Q_{SC} has a peak shape and I_{SC} has two sharp peaks. With increasing d, the maximum Q_{SC} and V_{OC} first increases and then decreases. And the maximum value of I_{SC} also has the same tendency. Figure 3d shows the maximum power with respect to the resistance for various d, which are obtained from the dynamic output curves (Figure S2, an example of d = 3.5 cm). It can be seen that the peak value of power has a first rise and a subsequent drop. The dependency of generated electric energy on the ball size is similar (Figure 3e). That is to say there exists an optimum ball size to reach the maximum power and energy. For a smaller ball, although it can get a larger initial velocity before its collision with TENG, due to longer moving distance, the larger deceleration ascribed to the smaller mass leads to a slower compression and a smaller deformation depth. The ball mass dominates the output power and electric energy. As the ball becomes larger, the deceleration decreases, and the output increases. However, for a ball that is large enough, further increasing its size will induce a much smaller initial velocity because of the restricted moving space, and the output performance declines. The existence of optimum ball size to realize the maximum output is resulting from the competition between the ball mass and allowable moving space. In addition, for a fixed ball size (*e.g.*, d = 3.0 cm), the power and energy both increase with the increase of height h (Figure 3f), which is attributed to the increase of allowable moving space.

Triggered by the water wave motion, the device with anchored TENG walls and a metal ball will be raised at

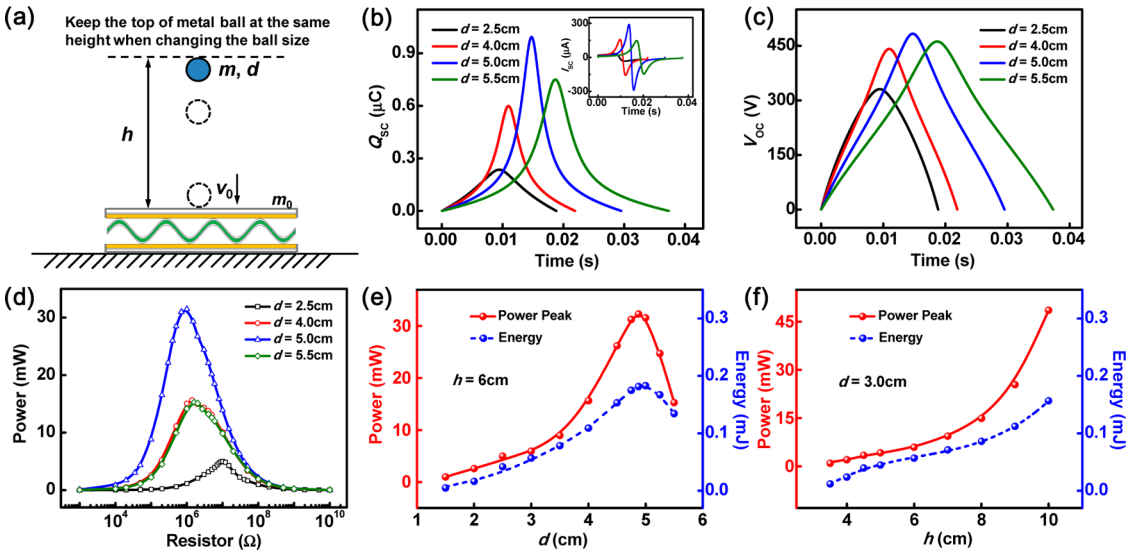

Figure 3. (a) Schematic representation of the vertical collision between the metal ball and TENG in the device. (b,c) Q_{SC}, I_{SC}, and V_{OC} as functions of time for various ball diameters d when given a constant height h = 6 cm. (d) Maximum output power with respect to the resistance for various d. (e) Effect of ball diameter on the maximum power and electric energy at a constant h. (f) Power and electric energy for various h at a fixed d (3.0 cm).

one end, and the sloping of device can induce the occurrence of collision.[22] To mimic the action of water waves, we designed the sloping collision mode as shown in Figure 4a. The sloping angle is defined as θ. The device is anchored on the ramp surface, and the ball is rolling from the acrylic surface of one TENG (zero initial velocity) to collide with the center of another TENG at an allowable moving length of L' = 6 cm. As well as above, the ball has the velocity v_0 and v_1 before its collision with the acrylic and after the collision. The component of gravity force of ball perpendicular to the ramp is offset by the normal force of the ramp, and the component along the ramp will act on the acrylic and wave-structured core. In this collision mode, the equations of $v(t)$ and $x_1(t)$ can be obtained by simply substituting $g\sin\theta$ for g in the vertical collision, and then the dynamic output characteristics can be calculated (Sections 1, 2 in Supporting Information).

The influences of ball size on the maximum output power and generated electric energy were examined for $\theta = 30°$. The results are presented in Figure 4b,c. The curves of power *versus* R for various d indicate that the increase of d can result in an increase of power peak value first, and then a decrease. Similar to Figure 3d, the power is first dominated by the mass of ball and then by the allowable moving space. The peak value of power can reach the maximum value at d = 3.5 cm under the currently adopted conditions. The optimum ball size (d = 5 cm) is also observed for the electric energy under the competition between ball mass and allowable moving space. Then we also calculated the sloping angle dependent output behavior for d = 3.5 cm (Figure 4d). It can be found that the power and energy both increase with increasing the sloping angle, implying that the larger wave height, the higher output. In addition, the number of metal balls may also have an impact on the output performance of TENG. But in a real device, the randomicity of moving orbit of metal balls or their mutual collision will bring the great complexity of output behavior. If the metal balls are restricted to move synchronously in a specific orbit with their mutual collision or separation prevented, the TENG impacted by the ball group can exhibit a stable output behavior. On the basis of this assumption, the relationships of peak power, electric energy and number N of metal balls were theoretically calculated for L' = 15 cm, d = 3.0 cm, and $\theta = 15°$ by regarding the balls as a group. Figure 4e shows the maximum power as a function of resistance for various N, and Figure 4f shows the power peak value and electric energy with respect to N. The power has the maximum value for two balls, and electric energy has the maximum for three balls. There exists an optimum ball number, but this conclusion is only correct based on the assumption.

In the calculations, a solid ball made of stainless steel was considered, for which the increase of mass is induced by the increase of size. If the ball is hollow with variable void ratios or it is made of different materials, the ball mass is variable for a fixed ball size. We calculated the maximum output power and generated electric energy of TENG for different ball masses at a fixed ball diameter (d = 3.0 cm) in the vertical collision and sloping collision modes. The results indicate that the power and energy increase with increasing the mass (Figure S3), which is due to the faster compression and the larger deformation depth for a larger mass at a constant allowable moving space. When the ball mass is large enough, the compression can last until

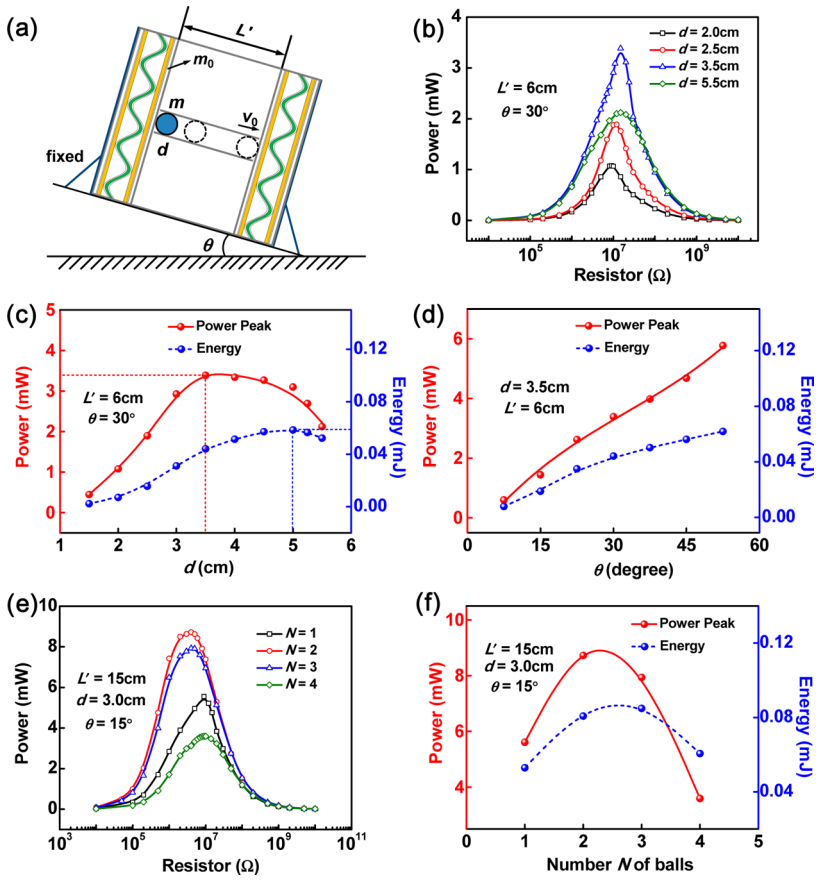

Figure 4. (a) Schematic representation of the sloping collision between the metal ball and TENG in the device. (b) Maximum output power with respect to resistance for various d at a moving length $L' = 6$ cm, and a sloping angle $\theta = 30°$. (c) Effect of ball size on the maximum power and electric energy at constant L' and θ. (d) Power and electric energy for various θ at fixed d (3.5 cm) and L' (6 cm). (e) Maximum output power with respect to resistance for various ball numbers N at $L' = 15$ cm, $d = 3.0$ cm, and $\theta = 15°$. (f) Effect of ball number on the maximum power and electric energy.

the complete contact, ensuring a high output performance of the TENG, but a too heavy ball is inadvisable. In addition, the thickness of the intermediate wavy dielectric film can have an influence on the TENG's output during the collision process. The wavy core is regarded as a harmonic spring, and its thickness affects the elastic force. As the thickness of the wavy dielectric film increases, the elastic force increases, and the film becomes more difficult to be compressed, thus the spring constant increases. This will lead to a slower compression and a smaller deformation depth, thereby a lower electric output. For two extreme cases, a too thick film largely increases the compression difficulty, and a too thin film cannot support the TENG to recover to its initial state. Therefore, a moderate film thickness is desirable for the TENG to generate a stable high output. The effect of the wavy film thickness will be examined carefully in our future study.

The above calculation results provide a theoretical prediction for the performance improvement of TENG in wave energy harvesting. To verify the theoretical results, we carried out the corresponding experiments including vertical collision and real water wave tests. The wavy-structured TENGs composed of a wavy Cu-Kapton-Cu film sandwiched between two fluorinated ethylene propylene (FEP) thin films coated by Cu were fabricated (Figure S4a). The detailed fabrication method can be found in the Methods section. To increase the surface charge of FEP and improve the TENG performance, electrons were first injected to the top surface of FEP film with Cu on its backside using the method in the literatures.[28,29] The wavy-structured TENG has been proved to be extremely stable and robust, and it is promising for water wave energy harvesting.

First, similar to Figure 3, we designed the vertical collision experiments (sketch is shown in Figure S4b), in which we also kept the top of metal ball at the same height (5.5 cm above the acrylic surface) to consider the restricted moving space. We measured the open-circuit voltage and short-circuit current of TENG during the collision between the ball and TENG for various ball sizes, as presented in Figure 5a,b. It can be found that as the metal ball becomes larger, the voltage and current first both increase, then reach saturations, and finally decrease. Note that the AC signal of current is because the wavy-structured core is self-restorable, while the AC signal of voltage results from the measurement

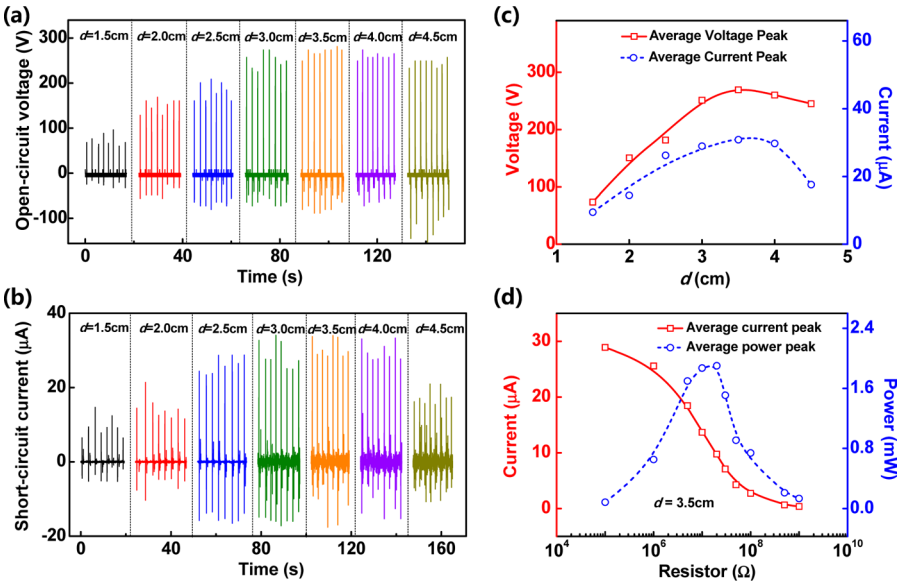

Figure 5. (a) Open-circuit voltage, (b) short-circuit current for various ball sizes in the vertical collision experiments. (c) Relationship between average voltage peak and current peak values and ball size. (d) Average peak current and power with respect to the resistance for the optimum ball diameter (d = 3.5 cm).

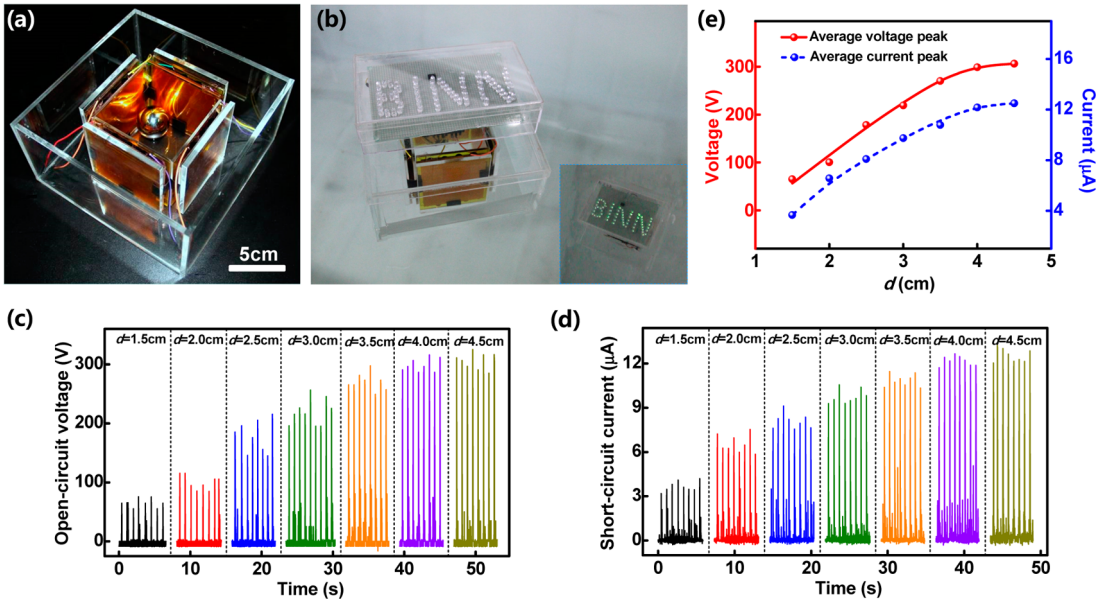

Figure 6. (a) Photograph of an as-fabricated TENG device for harvesting water wave energy. (b) Photograph of the device floating on water and optical images of 70 LEDs driven by the water wave. (c) Open-circuit voltage, (d) short-circuit current for various ball sizes in the water wave tests. (e) Relationship between average voltage peak and current peak values and ball size.

principle of digital oscilloscope. Figure 5c clearly shows that there exists an optimum ball size for the voltage and current to get the maximum average peak values. The result is in good agreement with the theoretical predictions as shown in Figure 3. Under the adopted conditions, the optimum ball diameter is 3.5 cm. For this optimum size, the TENG can transit an instantaneous power of 1.94 mW at the matched resistance of 20 MΩ (Figure 5d).

To further demonstrate the influence of ball size on the electric output for effective wave energy harvesting, four basic wavy-structured TENG units, standing anchored walls, allow a metal ball to form the single unit of TENG network, as the photograph shows in Figure 6a. The fabrication details are described in the experimental section. A photo of sealed device floating on water in a pool connected with scores of LEDs is shown in Figure 6b. Triggered by the water wave motion, these LEDs can be lightened up (see the inset). A video named as Video S1 was also captured to demonstrate the capacity of the device to harvest water wave energy. It is known that under the action of water waves, the device sloping induced collision drives the generation of electricity. According to Small

Amplitude Wave Theory,[30] a floating object or a water mass point experiences an elliptical trajectory under shallow water and a circular trajectory under deep water in a single-frequency cosine wave (Figure S5). The bobbing up and down of the device results in the collision between metal ball and TENGs. In fact, the real water waves in ocean are the group of waves with different frequencies, heights, and wavelengths; therefore, the motion of the device in ocean may be random. As long as the collision can occur, the device can work well. However, for better water wave conversion, an effective wave management to get regular waves is necessary in the future research.

In the following experiments, we adopted a single and constant wave condition to study the effect of the ball size on the electric properties. Similar to our previous work,[22] the seesawing motion of the tank with water inside at fixed amplitude and frequency will generate the water wave for experimental measurement. The open-circuit voltage and short-circuit current for various ball sizes were displayed in Figure 6c,d. Enlarged views of output for d = 3.5 cm in Supporting Figure S6 shows the bimodal character of current signal due to the restorability of wavy core. When the diameter of the metal ball tested increases from 1.5 to 4.5 cm, the voltage and current for balls with 1.5, 2.0, 2.5, 3.0, and 3.5 cm diameter increase dramatically with the increase of d, but voltage and current for 4.0 and 4.5 cm balls show a saturation tendency. The tendencies of average voltage and current peak values with respect to the ball diameter can be seen in Figure 6e. There exists an optimum ball diameter providing the maximized output, similar to above theoretical result. If the ball diameter can be increased further, the output will be decreased due to the competition between ball mass and allowable moving space according to above theoretical analysis. But we should note that if the metal ball becomes further larger, the acrylic box is easy to tilt seriously on the water surface, and the ball is very difficult to move due to the great sinking induced by the heavy ball. Otherwise, this work provides an approach of structural optimization for the TENGs toward water wave energy harvesting. After the TENGs with the optimized performance are integrated into the TENG network, the output performance of this network will be improved evidently. The TENG technology will play a more important role in current development of blue energy harvesting.

CONCLUSION

In summary, we have studied and optimized a basic unit of TENG network for harvesting water wave energy, which has a box structure composed of walls made of a wavy-structured Cu-Kapton-Cu film and two FEP thin films, with a metal ball enclosed inside. The theoretical model of the wavy-structured TENG was established, and its output characteristics when imposed a periodic triggering at a low frequency and a collision with the metal ball in typical collision modes were theoretically calculated. The results indicate that there exists an optimum ball size, mass, or number to reach maximized output power and electric energy. That provides a theoretical prediction for performance improvement of TENG in water wave energy harvesting. Then real water wave experiments were carried out using as-fabricated TENG devices to demonstrate the influence of ball size on the output performance, and a good agreement with the theoretical results was obtained. On the basis of the theoretical and experimental studies, this work could provide useful guidance for structural optimization of wavy-structured TENGs for effectively harvesting water wave energy.

METHODS

Fabrication of the Wave-Structured TENGs. First, a 125 μm thick Kapton film was periodically bent into a wavy shape by using a set of glass rods with diameter of 6 mm. The set was sent into a furnace and baked at 360 °C for 2 h. Because the Kapton film is thermoplastic, it can remain in the wavy shape stably below its glass transition temperature.[21] Then 200 nm thick copper was sputtered on both sides of the wavy Kapton film as electrodes. Second, two 20 μm thick FEP films (the type of FEP140 with $M_w \approx 432\,000$, purchased from DuPont Company) cleaned by the alcohol, acetone and deionized water in sequence, were deposited with a layer of copper on one side as the electrode. The copper sides of two FEP-Cu films were tightly attached to two acrylic substrates (with a size of 10 cm × 10 cm for vertical collision tests, while 8 cm × 8 cm for water wave tests). By placing a needle above the FEP surface of FEP-Cu film with a height of 5 mm, connecting the needle to the cathode, and connecting the Cu electrode to the anode and ground, electrons were injected to the top surface of FEP film. A polarization voltage of 5 kV was applied for 5 min. Third, by sandwiching the wavy Cu-Kapton-Cu film using two acrylic substrates with FEP films facing inside and bonding the structures together with adhesive tape, the wavy-structured TENG device was finally obtained.

For the water wave harvesting, four wavy-structured TENG units were vertically anchored onto the internal surface of acrylic plates in the center position of an acrylic box. The four TENGs were connected to a rectifier bridge and then connected in parallel. A steel ball was placed in the center of the device, and then the waterproofing was processed. When studying the effect of ball size, we placed a ball with the diameter of 1.5, 2.0, 2.5, 3.0, 3.5, 4.0, or 4.5 cm into the box center, respectively, and sealed the acrylic devices. Each device is the single unit of the TENG network for wave energy harvesting.

Electrical Measurement of the TENGs. The output voltage and current signals of the devices were measured by a digital oscilloscope (Agilent InfiniiVision 2000X) and a current preamplifier (Keithley 6514 System Electrometer).

Conflict of Interest: The authors declare no competing financial interest.

Acknowledgment. Support from the "thousands talents" program for the pioneer researcher and his innovation team,

China, and National Natural Science Foundation of China (Grant No. 61405131) are appreciated.

Supporting Information Available: The Supporting Information is available free of charge on the ACS Publications website at DOI: 10.1021/acsnano.5b06372.

Determination of x_1-t relationship and dynamic output characteristics of TENG during the collision between TENG and a metal ball, and experimental vertical collision and water wave tests. (Figure S1) Dynamic output performance at different load resistances during the horizontal collision; (Figure S2) dynamic output performance during the vertical collision; (Figure S3) effect of ball mass on the output performance for a fixed ball size; (Figure S4) sketch of wavy-structured TENG and the vertical collision experiment; (Figure S5) schematical diagram of moving trajectory of TENG device under the action of a single-frequency cosine wave; (Figure S6) enlarged view of the open-circuit voltage and short-circuit current in the water wave test. (PDF)
Movie S1. (AVI)

REFERENCES AND NOTES

1. Khaligh, A.; Onar, O. C. *Energy Harvesting: Solar, Wind, and Ocean Energy Conversion Systems*; CRC Press: Boca Raton, FL, 2009.
2. Falcao, A. F. de O. Wave Energy Utilization: A Review of the Technologies. *Renewable Sustainable Energy Rev.* **2010**, *14*, 899–918.
3. Wang, Z. L.; Chen, J.; Lin, L. Progress in Triboelectric Nanogenerators as a New Energy Technology and Self-Powered Sensors. *Energy Environ. Sci.* **2015**, *8*, 2250–2282.
4. Salter, S. H. Wave Power. *Nature* **1974**, *249*, 720–724.
5. Falnes, J. A Review of Wave-Energy Extraction. *Mar. Struct.* **2007**, *20*, 185–201.
6. Jouanne, A. V. Harvesting the Waves. *Mech. Eng. Mag.* **2006**, *128*, 24–27.
7. Henderson, R. Design, Simulation, and Testing of a Novel Hydraulic Power Take-Off System for the Pelamis Wave Energy Converter. *Renewable Energy* **2006**, *31*, 271–283.
8. Wolfbrandt, A. Automated Design of a Linear Generator for Wave Energy Converters-A Simplified Model. *IEEE Trans. Magn.* **2007**, *42*, 1812–1819.
9. Fan, F. R.; Tian, Z. Q.; Wang, Z. L. Flexible Triboelectric Generator. *Nano Energy* **2012**, *1*, 328–334.
10. Tang, W.; Jiang, T.; Fan, F. R.; Yu, A. F.; Zhang, C.; Cao, X.; Wang, Z. L. Liquid-Metal Electrode for High-Performance Triboelectric Nanogenerator at an Instantaneous Energy Conversion Efficiency of 70.6%. *Adv. Funct. Mater.* **2015**, *25*, 3718–3725.
11. Zhu, G.; Zhou, Y. S.; Bai, P.; Meng, X. S.; Jing, Q.; Chen, J.; Wang, Z. L. A Shape-Adaptive Thin-Film-Based Approach for 50% High-Efficiency Energy Generation through Micro-Grating Sliding Electrification. *Adv. Mater.* **2014**, *26*, 3788–3796.
12. Wang, S. H.; Lin, L.; Wang, Z. L. Triboelectric Nanogenerators as Self-Powered Active Sensors. *Nano Energy* **2015**, *11*, 436–462.
13. Xie, Y. N.; Wang, S. H.; Niu, S. M.; Lin, L.; Jing, Q. S.; Yang, J.; Wu, Z. Y.; Wang, Z. L. Grating-Structured Freestanding Triboelectric-Layer Nanogenerator for Harvesting Mechanical Energy at 85% Total Conversion Efficiency. *Adv. Mater.* **2014**, *26*, 6599–6607.
14. Lin, L.; Xie, Y. N.; Niu, S. M.; Wang, S. H.; Yang, P.-K.; Wang, Z. L. Robust Triboelectric Nanogenerator Based on Rolling Electrification and Electrostatic Induction at an Instantaneous Energy Conversion Efficiency of $\sim$ 55%. *ACS Nano* **2015**, *9*, 922–930.
15. Wang, S. H.; Xie, Y. N.; Niu, S. M.; Lin, L.; Wang, Z. L. Freestanding Triboelectric-Layer-Based Nanogenerators for Harvesting Energy from a Moving Object or Human Motion in Contact and Non-Contact Modes. *Adv. Mater.* **2014**, *26*, 2818–2824.
16. Wang, S. H.; Niu, S. M.; Yang, J.; Lin, L.; Wang, Z. L. Quantitative Measurements of Vibration Amplitude using a Contact-Mode Freestanding Triboelectric Nanogenerator. *ACS Nano* **2014**, *8*, 12004–12013.
17. Han, C. B.; Du, W. M.; Zhang, C.; Tang, W.; Zhang, L. M.; Wang, Z. L. Harvesting Energy from Automobile Brake in Contact and Non-Contact Mode by Conjunction of Triboelectrication and Electrostatic-Induction Processes. *Nano Energy* **2014**, *6*, 59–65.
18. Bae, J.; Lee, J.; Kim, S.; Ha, J.; Lee, B.-S.; Park, Y.; Choong, C.; Kim, J.-B.; Wang, Z. L.; Kim, H.-Y.; *et al.* Flutter-Driven Triboelectrification for Harvesting Wind Energy. *Nat. Commun.* **2014**, *5*, 4929.
19. Su, Y. J.; Wen, X. N.; Zhu, G.; Yang, J.; Chen, J.; Bai, P.; Wu, Z. M.; Jiang, Y. D.; Wang, Z. L. Hybrid Triboelectric Nanogenerator for Harvesting Water Wave Energy and as a Self-Powered Distress Signal Emitter. *Nano Energy* **2014**, *9*, 186–195.
20. Zhu, G.; Su, Y. J.; Bai, P.; Chen, J.; Jing, Q. S.; Yang, W. Q.; Wang, Z. L. Harvesting Water Wave Energy by Asymmetric Screening of Electrostatic Charges on a Nanostructured Hydrophobic Thin-Film Surface. *ACS Nano* **2014**, *8*, 6031–6037.
21. Wen, X. N.; Yang, W. Q.; Jing, Q. S.; Wang, Z. L. Harvesting Broadband Kinetic Impact Energy from Mechanical Triggering/Vibration and Water Waves. *ACS Nano* **2014**, *8*, 7405–7412.
22. Chen, J.; Yang, J.; Li, Z. L.; Fan, X.; Zi, Y. L.; Jing, Q. S.; Guo, H. Y.; Wen, Z.; Pradel, K. C.; Niu, S. M.; *et al.* Networks of Triboelectric Nanogenerators for Harvesting Water Wave Energy: A Potential Approach toward Blue Energy. *ACS Nano* **2015**, *9*, 3324–3331.
23. Jiang, T.; Chen, X.; Han, C. B.; Tang, W.; Wang, Z. L. Theoretical Study of Rotary Freestanding Triboelectric Nanogenerators. *Adv. Funct. Mater.* **2015**, *25*, 2928–2938.
24. Niu, S. M.; Liu, Y.; Wang, S. H.; Lin, L.; Zhou, Y. S.; Hu, Y. F.; Wang, Z. L. Theory of Sliding-Mode Triboelectric Nanogenerators. *Adv. Mater.* **2013**, *25*, 6184–6193.
25. Niu, S. M.; Liu, Y.; Wang, S. H.; Lin, L.; Zhou, Y. S.; Hu, Y. F.; Wang, Z. L. Theoretical Investigation and Structural Optimization of Single-Electrode Triboelectric Nanogenerators. *Adv. Funct. Mater.* **2014**, *24*, 3332–3340.
26. Niu, S. M.; Liu, Y.; Chen, X.; Wang, S. H.; Zhou, Y. S.; Lin, L.; Xie, Y. N.; Wang, Z. L. Theory of Freestanding Triboelectric-Layer-Based Nanogenerators. *Nano Energy* **2015**, *12*, 760–774.
27. Niu, S. M.; Wang, S. H.; Lin, L.; Liu, Y.; Zhou, Y. S.; Hu, Y. F.; Wang, Z. L. Theoretical Study of Contact-Mode Triboelectric Nanogenerators as an Effective Power Source. *Energy Environ. Sci.* **2013**, *6*, 3576–3583.
28. Wang, S. H.; Xie, Y. N.; Niu, S. M.; Lin, L.; Liu, C.; Zhou, Y. S.; Wang, Z. L. Maximum Surface Charge Density for Triboelectric Nanogenerators Achieved by Ionized-Air Injection: Methodology and Theoretical Understanding. *Adv. Mater.* **2014**, *26*, 6720–6728.
29. Eguchi, M. XX. On the Permanent Electret. *Philos. Mag.* **1925**, *49*, 178–192.
30. Newman, J. N. *Marine Hydrodynamics*; MIT Press: Cambridge, MA, 1978.